Comparative small-signal evaluation of advanced grid-forming control techniques

D.A. Aragon[1*], E. Unamuno[2], S. Ceballos[1], J. A. Barrena[2]

[1]Tecnalia, Basque Research and Technology Alliance (BRTA), Parque Tecnológico de Bizkaia, 48160 Derio, Spain

[2]Electronics and Computer Science Department, Mondragon Unibertsitatea, Faculty of Engineering, Mondragon, Spain

*Corresponding author (E-mail: diego.aragon@tecnalia.com)

Keywords

Grid-forming control, Inertia emulation, Low-inertia power systems, Synchronous machine emulation, Small signal analysis.

Abstract

This paper presents the small-signal modelling and analysis of the most recent grid-forming control techniques, namely the matching control (MC) and the dispatchable virtual oscillator (dVOC). These are compared to more classical SME techniques such as synchronverters (SV) and voltage-controlled virtual synchronous machines (VCVSM) under different grid conditions. In addition to studying the time-domain response (inertial behaviour, steady-state operation point, etc.), a thorough evaluation of the dominant eigenvalues of each control is carried out by obtaining the participation factors and the sensitivity to physical and control parameter variations. Simulation results are obtained for a grid-forming converter connected to a dynamic grid model that emulates different properties of low-inertia power systems—e.g. primary reserve, inertial strength, coupling strength, etc. Besides, hardware-in-the-loop experimental results are presented to validate the analysis.

1 Introduction

Due to the political and economic changes caused by global warming, more and more renewable energy systems (RES) and energy storage systems (ESS) are being integrated into electric power systems. Most of the time, these systems are connected to the grid by power converters. However, one of the main challenges to massively connect converters to the network is that—unlike classical synchronous machines with big inertia—they do not inherently respond under voltage or frequency variations [1]. Additionally, converters introduce much faster dynamics than synchronous machines, which may cause interoperability problems affecting the frequency and voltage regulation [2]. In response to these challenges, one of the solutions proposed by the research community is to control converters as grid-forming converters (GFM). Their main advantage is that they can support the power

system under normal, disturbed, and emergency conditions, since the converter sets the frequency and voltage at the connection node.

In recent years, a full range of control techniques have been proposed to contribute to the regulation of the grid [3], starting from the droop control classically employed to regulate the speed of synchronous machines [4], to synchronous machine emulation (SME) techniques [5] which incorporate the swing equation of a synchronous machine in the controller to deliver a synthetic inertial response under power imbalances. A more recent example is the so-called matching control (MC) [6], which takes advantage of the physics of the converter to deliver the energy stored in the dc-link in the event of changes in the grid frequency. Another recent approach is the dispatchable virtual oscillator (dVOC) [7], which guarantees almost global asymptotic stability for converter-based networks [8].

To correctly integrate these new control strategies into the power grid, it is necessary to ensure the system's proper operation in steady state and transient regimes. In this context, the small-signal analysis is one of the most used techniques to assess the dynamic behaviour of conventional networks and the stability with a high integration of RES, since it allows to identify the location of the eigenvalues in the complex plane. In the field of grid-forming converters, the assessment of the small-signal stability has been used, e.g., to compare the equivalence of a virtual synchronous machine and the droop control, concluding that they are equivalent from the perspective of stability [9]. Another study analyses the SME techniques implemented with dynamic and quasi-dynamic models [10], while others compare their behaviour against classical synchronous machines (SM) [5, 11]. Nevertheless, when assessing the stability of the system, these studies model the grid as a single-machine, infinite-bus system with a fixed frequency.

The gradual integration of GFM converters in the grid has caused the necessity to employ grid models that consider dynamic variations of the frequency under power perturbations. In [12], for instance, the eigenvalues of a GFM-based network are studied and sensitivity analyses are carried out by considering load and line dynamics and GFM converters with internal voltage and current loops. Similarly, in [2] a small-signal study of a droop-based GFM converter connected to a dynamic grid model is carried out, where the dynamics of transmission lines are also included. In [13] the frequency stability of a SM and various GFM control approaches are discussed, but the study is limited to time-domain simulations.

This paper aims to benchmark the small-signal properties of MC and dVOC control techniques against well-established SME strategies synchronverters (SV) and voltage-controlled virtual synchronous machines (VCVSM), taking into account the internal voltage and current loops. To this date, most small-signal stability studies have either considered the power system to be a stiff voltage source, or have been focused on a single control strategy. This manuscript aims to go one step further by evaluating and comparing the behaviour of several grid-forming (GFM) control strategies under different grid types and conditions. For that purpose, the GFM converter is connected to an equivalent low-inertia grid model capable of emulating different levels of aggregated inertia, damping, and lines impedances [2, 14, 15]. In addition to evaluating the time-domain response of the four GFM controllers, several parametric sensitivity analyses are carried out to reveal the inherent small-signal properties of the controllers and to evaluate their performance under different grid conditions.

The operation points have been first analysed through time-domain simulations. Then, small-signal models are obtained to compare the critical modes, participation factors and parameter sensitivity of the GFM control parameters. After that, the dynamic properties of the controllers under different load variations, equivalent grid impedance, total inertia and level of converter penetration are analysed.

The results of the study have been experimentally corroborated by means of real-time hardware-in-the-loop (HIL) tests, where the controllers are implemented in an external Texas Instruments F28739D launchpad control hardware.

The rest of the document is structured as follows: Section 2 contains the description and the small-signal modelling of the use case, including the mathematical formulation of the power converter and the inner voltage and current loops. Section 3 presents a brief overview of each control technique, and the dynamic performance tests and validation of the models are included in Section 4. Section 5 contains a parametric sensitivity analysis of the control techniques for different grid conditions, and Section 6 includes the real-time validation in the HIL platform. Finally, Section 7 provides the most relevant conclusions and remarks of the study.

2 Use case modelling

In this section, a description of the scenario under study and the mathematical formulation of the converter and the equivalent grid model is included.

2.1 General system description

The scenario shown in Figure 1 consists of a GFM converter connected to a low-inertia power system. Unlike in other studies where the grid is considered to be stiff, in this case the grid model is based on a simplified synchronous machine. The purpose of this non-stiff grid model is to emulate several grid conditions and grid types by representing different levels of aggregated inertia, damping or line impedances. It must be noted that this type of equivalent grid model is valid as long as the system dynamics are dominated by the electromechanical oscillations of synchronous generators and/or GFM converters connected to that grid. If the inertial response of the simplified grid was extremely low, the model would have to be adapted to also represent faster oscillations caused by transmission lines and inner control loops of grid-connected devices. The mathematical foundations of this model are explained in Section 2.2.

In addition to the GFM control algorithm, the converter model includes the output *LC* filter and inner current and voltage loops. Moreover, the dc-link capacitor dynamics and its regulation are also considered in this study. The details of this model are explained in Section 2.3.

To ensure the correct operation of the system, the converter dynamics are adjusted to satisfy the time scales of the synchronous machines.

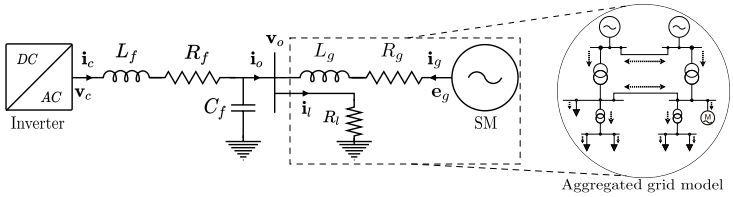

Fig. 1: One-bus system comprised of GFM and aggregated grid model

2.2 Aggregated grid model

The electromagnetic behaviour of the aggregated grid model is represented by a simplified synchronous machine model that takes into account the dynamics of a governor and a turbine (Figure 2).

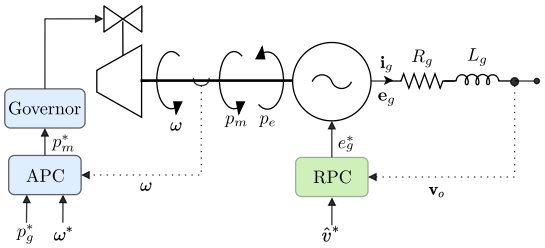

Fig. 2: Synchronous generator model.

The electromechanical behaviour of the grid frequency is represented by the swing equation (ω) [16]:

$$\dot{\omega} = \left[p_m - p_e - k_{d_g}(\omega - \omega^*)\right] \frac{1}{2H_g} \tag{1}$$

where p_e and p_m are the electrical and mechanical power, respectively. k_{d_g} is the damping constant of the frequency, H_g the inertia constant and ω^* is the frequency reference.

The mechanical power is established by an aggregated turbine model, which in this case is modelled as a first-order transfer function:

$$\dot{p}_m = \frac{1}{t_t}(g - p_m) \tag{2}$$

where t_t represents the time constant of the equivalent turbine.

The input flow g of this equivalent turbine is dependent on the governor, which has been also modelled as a first-order transfer function:

$$\dot{g} = \frac{1}{t_g}(p_m^* - g) \tag{3}$$

where t_g is the time constant of the governor.

The mechanical power reference p_m^* is calculated with a p/ω droop regulator as follows:

$$p_m^* = p_g^* + k_{\omega_g}(\omega^* - \omega) \tag{4}$$

where p_g^* is the output power reference.

The electrical behaviour of the grid currents is represented as a series *RL* impedance, given by:

$$\dot{\mathbf{i}}_g = \frac{\omega_b}{L_g}\left[\mathbf{e}_g - \mathbf{v}_o - (R_g + j\,\omega L_g)\,\mathbf{i}_g\right] \tag{5}$$

where L_g and R_g are the equivalent grid-side inductance and resistance, respectively. $\mathbf{e}_g$ is the vector representing the voltage of the grid, which is controlled via a reactive power control (RPC).

The RPC generates the voltage reference with a q/v droop controller with gain k_v:

$$e_s^* = \hat{v}_o^* + k_v\left(q_g^* - q_g\right) \tag{6}$$

where $\hat{v}_o^*$ is the voltage reference.

The grid voltage components are obtained as:

$$e_{s_d} = e_s^* \quad e_{s_q} = 0$$

2.3 Inverter with *LC* filter and inner loops

The dc-ac inverter model employed is a detailed representation of an average model represented in the synchronous reference frame (SRF) as shown in Figure 3.

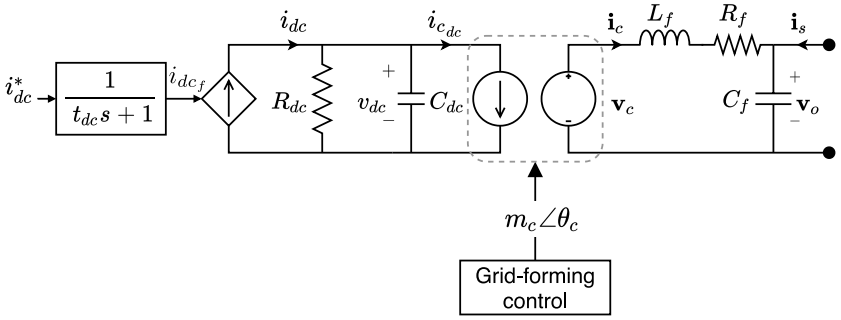

Fig. 3: Converter model in SFR.

L_f, R_f and C_f are the inductance, series resistance and capacitance of the output filter of the converter, respectively. The current flowing through the filter inductor is modelled as follows:

$$\dot{\mathbf{i}}_c = \frac{\omega_b}{L_f}\left[\mathbf{v}_c - \mathbf{v}_o - \left(R_f + j\,\omega L_f\right)\mathbf{i}_c\right] \tag{7}$$

where ω_b is the base frequency for the per-unit representation and ω is the frequency of the SRF. Vector notation with boldfaced symbols is used to represent variables that contain d- and q-axis components, e.g., $\mathbf{i_c} = i_{c_d} + j i_{c_q}$.

Since the inverter is represented with an average model, the converter output voltage $\mathbf{v}_c$ depends on the modulation index ($\mathbf{m}_c$) as follows:

$$\mathbf{v}_c = \mathbf{m}_c\, v_{dc} \tag{8}$$

where v_{dc} is the dc bus voltage.

The voltage across the filter capacitor is modelled as:

$$\dot{\mathbf{v}}_o = \frac{\omega_b}{C_f}\left[\mathbf{i}_c - \mathbf{i}_o - j\,\omega C_f \mathbf{v}_o\right] \tag{9}$$

Most of the studies in the literature assume that the bus voltage of inverters is constant. However, to obtain a more accurate representation of the voltage dynamics, the dc-bus is represented by a capacitor C_{dc} and a parallel resistance R_{dc} that accounts for the converter losses. This representation allows taking into account the voltage variations of the dc-bus. The voltage across the dc-bus capacitor is expressed as follows:

$$\dot{v}_{dc} = \frac{\omega_b}{C_{dc}}\left[i_{dc} - i_{c_{dc}} - \frac{v_{dc}}{R_{dc}}\right] \tag{10}$$

where $i_{c_{dc}}$ is the dc-side converter current, which is obtained from the average inverter model as:

$$i_{c_{dc}} = \frac{v_{c_d}\, i_{c_d} + v_{c_q}\, i_{c_q}}{v_{dc}} \tag{11}$$

The dc current source, i_{dc}, is determined by a dc voltage control as proposed in [13]. This control is comprised by a proportional regulator and a feed-forward term of active power to compensate for the losses of the *LC* filter. The elimination of the steady-state error is taken into account to ensure correct synchronisation of the matching control and improve the voltage regulation of the rest of GFM approaches considered in this study:

$$i^*_{dc} = k_{dc}\,(v^*_{dc} - v_{dc}) + \frac{p^*}{v^*_{dc}} + \frac{v_{dc}}{R_{dc}} + \frac{p_c - p_o}{v^*_{dc}} \tag{12}$$

where k_{dc} is the proportional gain, p_c is the power passing through the converter, p_o is the power measured at the PCC, p^* is the reference of the output active power, v_{dc}/R_{dc} is the current that flows through the resistor R_{dc} that is added to compensate the losses on the dc side.

The generated current reference is then passed through a first-order filter that represents the dynamics of the dc bus current controller:

$$\dot{i_{dc_f}} = \frac{1}{t_{dc}}(i^*_{dc} - i_{dc_f}) \tag{13}$$

The grid-forming controllers considered in this study make use of the active and reactive power of the converter. These magnitudes are measured and then filtered with a first-order filter as shown in Figure 3. The output of the controller is the modulation index $\mathbf{m_c}$, which is used in the average model of the inverter.

The modulation index is determined by an inner control loop composed of a PI voltage regulator in cascade to a PI current regulator, to control the output voltage and currents of the *LC* filter, respectively (Figure 4). Although in the literature these internal loops have been treated mainly for the VCVSM, they are used in the SV, dVOC and MC in several studies because they provide a way to limit the voltage and current of the converter in the

controller [13, 17, 18].

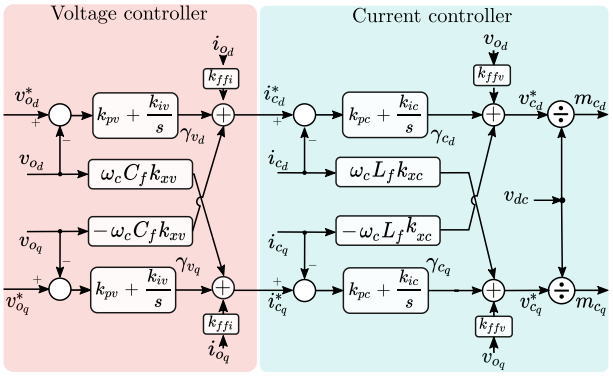

Fig. 4: Block diagram of the inner loops.

3 Overview of grid-forming control techniques

3.1 Synchronous machine emulation

SME techniques have gained relevance in recent years. These techniques integrate the mechanical model of classical synchronous machine- i.e., the swing equation shown in (1)— into the converter control as a way to provide similar damping and inertial response against power imbalances than synchronous machine. The voltage amplitude at the converter output terminals is determined by an electrical model of the emulated SM and an automatic voltage regulator (AVR). The main difference of SME techniques with regard to real synchronous machine is that the delays caused by the governor, turbine and exciter can be avoided or modulated, thus improving the dynamics of the response.

One of the main features of SME techniques is that, as they emulate the behaviour of synchronous machine, the operation principles of the power system are not drastically modified, thus ensuring the converters interact adequately with the rest of the grid components. There are multiple SME implementations in the literature, being the synchronverters and the voltage-controlled virtual synchronous machines some of the most widely used approaches [5].

3.1.1 Synchronverter

Synchronverters (SVs) are the most straightforward technique to mimic the behaviour of a classical synchronous machine, since they usually do not include any inner voltage/current loop, and they do not estimate the grid frequency with a synchronizing algorithm such as a phase-locked loop to determine the damping. Instead, it is assumed that the grid frequency is fixed in ω^*, avoiding the use of frequency estimators [19]. A streamlined version is shown in Figure 5.

A synchronverter, as other SMEs, is comprised by a frequency droop control with a gain k_ω and a damping term k_d. The control of the reactive power is usually carried out by a voltage droop control with gain k_q. The final

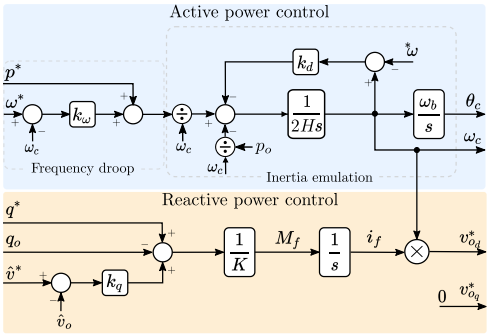

Fig. 5: Synchronverter block diagram.

reactive power reference is multiplied by a $1/K$ gain, integrated and multiplied by the angular speed to emulate the inner voltage of the synchronous machine.

3.1.2 Voltage-controlled virtual synchronous machine

Voltage-controlled virtual synchronous machines (VCVSM) have been widely studied in the literature [5, 9], and the typical structure of active and reactive power loops can be observed in Figure 6.

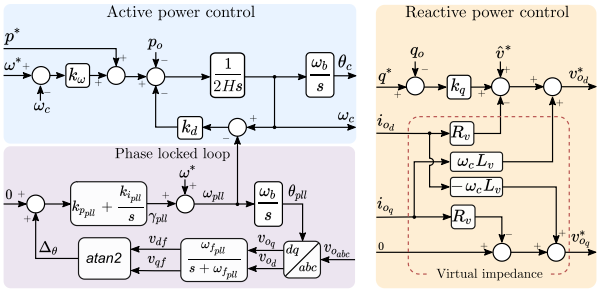

Fig. 6: Active and reactive control of the voltage-controlled virtual synchronous machine block diagram.

Compared to the SV, the higher number of control loops complicates the tuning of the control parameters, but at the same time it provides more degrees of freedom to adapt the dynamic behaviour of the converter. For the regulation of the active power, the controller includes a frequency droop with gain k_ω and the swing equation as in the SV. The difference is that VCVSMs also include a phase locked loop (PLL) to estimate the grid frequency that is used to calculate the damping term and a static virtual-impedance. The block diagram of the PLL shown in Figure 6 follows the same configuration as the one used in [9], but other PLL approaches are also valid. Regarding the reactive power regulation, VCVSMs employ a voltage droop with gain k_q.

3.2 Matching control

Matching control (MC) is a new control philosophy proposed initially in [20] and further studied in [6,21,22]. This control is different from classical SME techniques because it is based on the analogy between the rotor dynamics of synchronous machine (ω_r) and the dc-link voltage dynamics (v_{dc}) of two-level inverters. These equivalences

can be observed through the following expressions:

$$\underbrace{\dot{\omega}_r = \left[\frac{\tau_m}{\omega_r} - \frac{\tau_e}{\omega_r} - k_d(\omega_r - \omega^*)\right]\frac{1}{2H}}_{\text{SM}} \leftrightharpoons \underbrace{\dot{v}_{dc} = \frac{i_{dc}}{C_{dc}} - \frac{i_{c_{dc}}}{C_{dc}} - \frac{i_{R_{dc}}}{C_{dc}}}_{2-\text{level inverter}} \tag{14}$$

MC techniques are based on establishing a correlation between the speed of synchronous machine and the bus voltage as follows:

$$\dot{\theta}_c = \psi\, v_{dc}\, \omega_b = \omega_c\, \omega_b \tag{15}$$

where $\psi = \omega^*/v_{dc}^*$. Considering the analogy between the dynamic equations established in 14 and the correlation between speed and bus voltage in 15, it is possible to define the remaining parameters as $k_d = \psi^2/R_{dc}$, $T_m = i_{dc}/\psi$ and $T_e = i_{c_{dc}}/\psi$.

In other words, the MC uses the energy stored in the bus capacitor to release it when there is a power imbalance in the ac grid, while the power losses caused by R_{dc} behave as the damping term of the synchronous machine. Figure 7 shows a possible implementation of the MC. This control does not have a reactive power controller, but a PI regulator with $k_{p\hat{v}}$ and $k_{i\hat{v}}$ constants to control the voltage at the PCC.

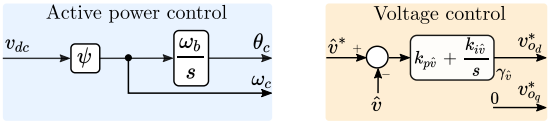

Fig. 7: Matching control diagram block.

In this technique, the converter that regulates the dc voltage acts as a governor, so the dc-link control has to be based on a droop regulator that allows power-sharing.

3.3 Dispatchable virtual oscillator control

The techniques described above were designed to operate electronic converters as a synchronous machine to maintain scaling times of a traditional power system. Nevertheless, the dispatchable virtual oscillator (dVOC) is based on the theory behind non-linear oscillators, allowing the synchronisation between converter-based networks. One notable feature of dVOC is its capability to rapidly stabilise the oscillator, i.e., reach the sinusoidal steady-state of the inverter output voltage from any initial condition [23].

Figure 8 illustrates the block diagram of a dVOC in rectangular coordinates and for an inductive system ($\kappa = \pi/2$), where active and reactive power control loops can be distinguished.

4 Model validation, performance tests and modal analysis

To analyse the small-signal behaviour of the control techniques presented in Section 3, the methodology implemented in [5], which consists of modelling, validation of the small-signal model, and evaluation of the dynamic behaviour in response to power reference changes and grid frequency variations, is followed.

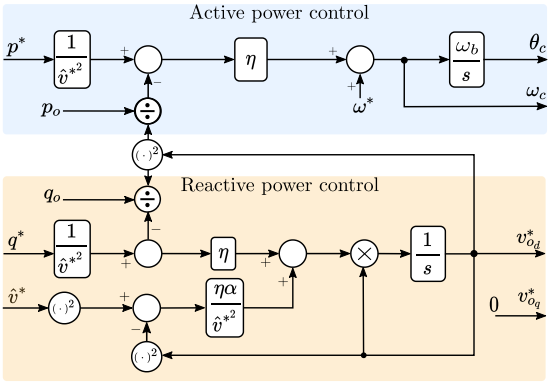

Fig. 8: Dispatchable virtual oscillator block diagram.

4.1 Small-signal modelling

The models of the generator, load, converter and each of the control approaches introduced in the previous section are first described via a set of differential-algebraic equations. The state vector of the system where the converter is controlled with an SV technique ($\mathbf{x}_{\text{SV}}$) contains 20 states, 29 states for the VCVSM ($\mathbf{x}_{\text{VCVSM}}$), 18 states for the MC ($\mathbf{x}_{\text{MC}}$) and 19 for the dVOC ($\mathbf{x}_{\text{dVOC}}$).

$$\mathbf{x}_{\text{SV}} = \left[i_{g_d}\, i_{g_q}\, \omega\, p_m\, g\, i_{c_d}\, i_{c_q}\, v_{o_d}\, v_{o_q}\, v_{dc}\, p_o\, q_o\, i_{dc}\, \gamma_{v_d}\, \gamma_{v_q}\, \gamma_{c_d}\, \gamma_{c_q}\, \omega_c\, \theta_c\, i_f\right]$$

$$\mathbf{x}_{\text{VCVSM}} = \left[i_{g_d}\, i_{g_q}\, \omega\, p_m\, g\, i_{c_d}\, i_{c_q}\, v_{o_d}\, v_{o_q}\, v_{dc}\, p_o\, q_o\, i_{dc}\, \gamma_{v_d}\, \gamma_{v_q}\, \gamma_{c_d}\, \gamma_{c_q}\, v_{dc}\, \gamma_{c_d}\, \gamma_{c_q}\, \gamma_{v_d}\, \omega_c\, \theta_c\, v_{df}\, v_{qf}\, \gamma_{pll}\, \theta_{pll}\right]$$

$$\mathbf{x}_{\text{MC}} = \left[i_{g_d}\, i_{g_q}\, \omega\, p_m\, g\, i_{c_d}\, i_{c_q}\, v_{o_d}\, v_{o_q}\, v_{dc}\, \theta_c\, p_o\, q_o\, i_{dc}\, \gamma_{\hat{v}}\, \gamma_{c_q}\, \gamma_{v_d}\, \gamma_{v_q}\, \gamma_{c_d}\right]$$

$$\mathbf{x}_{\text{dVOC}} = \left[i_{g_d}\, i_{g_q}\, \omega\, p_m\, g\, i_{c_d}\, i_{c_q}\, v_{o_d}\, v_{o_q}\, v_{dc}\, p_o\, q_o\, i_{dc}\, \gamma_{v_d}\, \gamma_{v_q}\, \gamma_{c_d}\, \gamma_{c_q}\, \theta_c\, v^*_{o_d}\right]$$

The input vector ($\mathbf{u}$) for the four cases is identical, and is defined as follows:

$$\mathbf{u} = \left[p^*_g\, v^*_{dc}\, q^*\, p^*\, \omega^*\, \hat{v}^*\right]$$

Some of the equations that describe the dynamics of these state variables are non-linear, meaning that they have to be linearized around an operating point to obtain their state-space matrix form. To obtain the operating point, the time derivatives are made equal to zero and the resulting system of equations are solved. The equations are then linearized by applying the Taylor series expansion to obtain the small-signal model given in the form:

$$\Delta\dot{\mathbf{x}} = \mathbf{A}\left(\mathbf{x}_0\right)\Delta\mathbf{x} + \mathbf{B}\left(\mathbf{x}_0\right)\Delta\mathbf{u} \tag{16}$$

where Δ represents the small signal variation and $\mathbf{x}_0$ is the operating point. The linearization process and the time-domain and eigenvalue analysis is carried out in the software CSTEP [24].

4.2 Parameter values

The system parameters and the default set-points are listed in Table I. The base power S_b is the power value employed to calculate all the system p.u. parameters and variables. In this case, it has been defined to be equal to the rated power of the inverter (2.75MVA). The rated power of the equivalent grid model is not explicitly defined, since all aggregated parameters (inertia, damping, series impedance, etc.) are defined according to the base power. By modifying these p.u. values, a more or less strong grid can be emulated with respect to the inverter. On the other hand, to provide a fair comparison and to guarantee the correct integration of the GFM converter in the system, the four control techniques are tuned to provide a similar steady-state and transient response (i.e., the rate of change of the output frequency or RoCoF). The methodology employed in [13] is used to adjust the droop gains of each technique. The internal voltage and current loops are the same for the four control strategies. The current loop parameters are designed with the modulus optimum criterion. The voltage loop and the PLL are tuned according to the symmetrical optimum criterion to ensure the maximum phase margin [25]. However, the k_{iv} gain of the voltage loop (see Figure 4) has been readjusted employing a parametric sweep.

Table I: Parameter values for the case study.

System general values					
S_b	2.750 MVA	v_b	690 V	ω_b	$2\pi 50$ rad/s
v_{dc_b}	1126.8 V				
Aggregated grid					
L_g	0.2 p.u.	R_g	0.016 p.u.	k_v	0.270
H_g	2 s	k_{d_g}	0	t_g	0.1 s
k_{w_g}	4.430	t_t	1 s	R_l	1 p.u.
Converter					
S_c	1 p.u.	R_{dc}	20 p.u.	C_{dc}	37.7 p.u.
C_f	0.078 p.u.	R_f	0.006 p.u.	L_f	0.08 p.u.
t_{dc}	0.066 s	f_{sw}	5.120 kHz		
Control set-points of the converter and aggregated grid					
v_{dc}^*	1 p.u.	$q*$	0 p.u.	p^*	0.5 p.u.
ω^*	1 p.u.	$\hat{v}^*$	1 p.u.	p_g^*	0.5 p.u.
Inner voltage and current loops					
k_{pv}	1.060	k_{pc}	1.3	k_{ffv}	1
k_{iv}	16	k_{ic}	30.7	k_{ffi}	1
MC					
ψ	1	$k_{p\hat{v}}$	0.4	$k_{i\hat{v}}$	5
k_{dc}	6.016	t_p	$31.8 \cdot 10^{-3}$ s		
dVOC					
η	0.204	α	0.4	κ	$\frac{\pi}{2}$
t_p	0.360 s	t_q	$5.263 \cdot 10^{-3}$ s		
SV					
k_d	12	H	2 s	K	1
k_ω	4.430	k_q	2	t_q	$5.263 \cdot 10^{-3}$ s
t_p	$4 \cdot 10^{-4}$				
VCVSM					
k_d	12	H	2 s	k_w	4.930
k_q	2	$k_{p_{pll}}$	0.050	$k_{i_{pll}}$	1
$\omega_{f_{pll}}$	500 rad/s	L_v	0.1 p.u.	R_v	0.050 p.u.
t_q	0.0370 s	t_p	$4 \cdot 10^{-4}$ s		

4.3 Model validation and performance tests

4.3.1 Active power reference variation

Figure 9 presents the behaviour of the linearized and non-linear model of the system described in Figure 1 for a variation in the active power reference of the converter of 0.1 p.u. The curves reveal that the linearized (small-signal) models and the original non-linear models coincide in their transient response for a step-shaped variation in the active power reference. The strong transient in the dVOC is due to this approach's disadvantage in adding synthetic inertia to the network without modifying the structure of the original control. Regarding the SV, the fluctuations have a frequency of oscillation which is very similar to that of the VCVSM. Nevertheless, the values of the SV in steady-state are different compared to the rest of GFM implementations because the damping factor term acts upon the virtual frequency and not the system frequency ($k_d(\omega_c - \omega^*)$). This might entail a disadvantage in grids where the SV plays a significant role in frequency regulation because it affects the power-sharing with respect to the rest of grid-forming systems. A different situation occurs with the VCVSM, which, by attaching the PLL to estimate the grid frequency and using it in the damping term, uncouples the effect of the damping and the droop and manages to take full advantage of this physical characteristic of synchronous machines to damp the oscillations in the power system. The MC exhibits a relatively clean and oscillation-free behaviour because its synchronisation is fast since the synthetic inertia delivered by the converter is limited by the size of the dc bus capacitor. These results also demonstrate that the small-signal models adequately represent the dynamics of the original models even for a significant deviation from the initial point of operation. Therefore, these small-signal models will be used to study further the oscillation modes and the influence of parameter variations in the following sections.

4.3.2 Load power variation

To analyse the frequency response against power imbalances, a change on the active power of the load (R_l in Figure 1) of 0.1 p.u. is assumed at $t = 2$s. Figure 10 a and b show the active power behaviour of the converter and the grid, respectively. As mentioned above, the SV damping term affects the steady-state of the grid, and in the event of variations in the system load, the SV tends to deliver more active power to the grid. In the other strategies, the active power has similar steady-state behaviour in each case; however, there are some small differences, primarily caused by each technique's type of reactive power regulation. Concerning the frequency behaviour, all cases show better damping of the oscillations than when the power reference is varied. Figure 10-c shows the frequency behaviour, where the techniques have a similar rate of change of frequency (RoCoF). Nevertheless, the MC exhibits a higher frequency drop with a steeper slope because the dc capacitor is insufficient to deliver the same synthetic inertia as the other techniques studied.

Figure 10-d depicts the voltage behaviour at the PCC. The dVOC achieves a fast and accurate voltage control while keeping load sharing capability. In comparison, the SV and VCVSM show a slight voltage drop, although the SV reaches steady-state more slowly due to the integrator and the division by K, which behaves like a low-pass

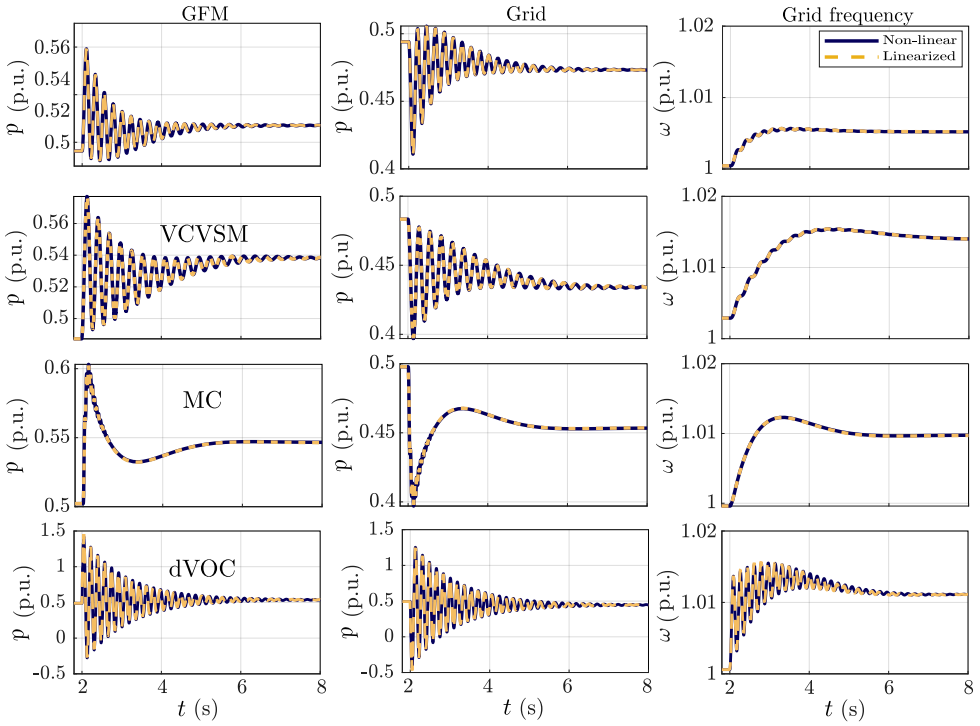

Fig. 9: Validation of small-signal models under active power reference variations. From left to right, GFM power, SM power and grid frequency in each case.

filter.

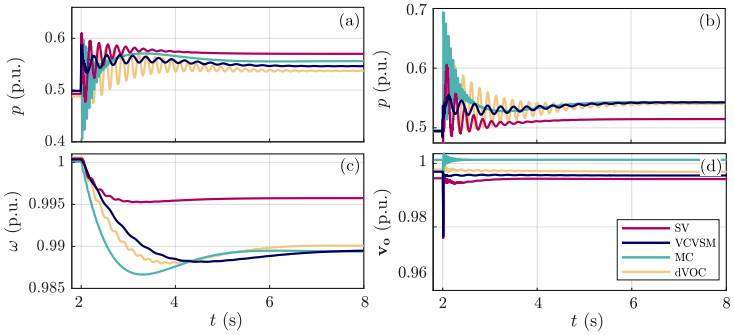

Fig. 10: Response against load variations of the lineal model. a) active power of the converter. b) Synchronous generator active power. c) Grid frequency. d) Voltage of the PCC.

4.4 Modal analysis

A popular technique to assess the stability of power systems is to analyse the eigenvalues of the matrix $\mathbf{A}$ of the linearized state-space model in (16). The properties of these eigenvalues provide helpful information about the system dynamics such as the damping factor, the sensitivity to parameter deviations, the relation between states and oscillation modes (via the participation factors) and the oscillation frequencies.

The properties of the most relevant eigenvalues for the investigated control techniques are gathered in Table II. Critical eigenvalues are defined as those with a real part greater than -15 and a damping ratio lower than 15%.

The modes that are most influenced by the grid-forming control reveal that the SME techniques present similar oscillation frequencies and damping factors. However, the VCVSM attenuates the oscillations better due to the

Table II: Critical eigenvalues and their most relevant information.

Case	Eigenvalue	ζ	f_{osc} (Hz)	Participating state	Parameter sensitivities
SV	$-0.99 \pm 28.05j$	0.03	4.46	$\theta_c\ \omega_c\ \omega$	$k_{ffi}\ R_f\ R_g\ H$
	$-1.39 \pm 0.62j$	0.91	0.09	$\tau_m\ \omega\ \omega_c$	$t_t\ t_g\ H_g\ H$
	-4.69	1	0	i_f	$k_v\ K\ k_q$
	$-5.66 \pm 25j$	0.21	4.20	$v_{dc}\ i_{dc}$	t_{idc}
	$-8.84 \pm 370j$	0.02	59	$i_{s_d} i_{s_q}\ i_{c_d}\ i_{c_q}$	$R_g\ k_{ffi}\ R_f$
	-10	1	0	g	t_g
VCVSM	$-0.74 \pm 0.74j$	0.70	0.1	$\tau_m\ \omega\ \omega_c$	$t_t\ t_g\ k_{d_g}\ H_g$
	$-0.81 \pm 22.49j$	0.03	3.60	$\theta_c\ \omega\ \omega_c$	$k_{p_{pll}}\ R_v\ k_{ffv}$
	$-5.68 \pm 25j$	0.21	4.20	$v_{dc}\ i_{dc}$	$t_{idc}\ C_{dc}$
	$-8.73 \pm 16j$	0.47	2.50	$\varepsilon_{pll}\ \theta_{pll}$	$k_{p_{pll}}$
	-10	1	0	g	t_g
	$-14.25 \pm 501j$	0.02	79	$i_{s_d}\ i_{s_q}$	$R_v\ k_{ffi}\ L_v$
MC	$-1.14 \pm 1.11j$	0.71	0.20	$\omega\ \tau_m$	$t_g\ t_t\ R_g$
	-3.57	1	0	γi_v	$k_{p_c}\ k_{ffi}\ k_{i_v}$
	$-5.96 \pm 123j$	0.04	19.7	$v_{dc}\ \theta_c$	$R_g\ k_{ffi}\ R_f$
	$-7.34 \pm 365j$	0.02	58	$i_{s_d}\ i_{s_q}$	$R_g\ k_{ffi}\ R_f$
	-10	1	0	g	t_t
	$-15.42 \pm 114j$	0.74	2.20	$p_o\ i_{dc}$	$k_{ffi}\ L_g\ R_f$
dVOC	$-0.92 \pm 36j$	0.02	5.73	$\theta_c\ p_o\ \omega$	$R_f\ k_{ffi}\ R_g$
	-0.60	1	0	$v^*_{o_d}$	$\eta\ k_v$
	$-0.87 \pm 0.90j$	0.70	0.10	$\tau_m\ \omega\ p_o$	$\eta\ t_g\ t_t$
	$-5.67 \pm 25.67j$	0.21	4.08	$v_{dc}\ i_{dc}$	$t_{idc}\ C_{dc}$
	-10	1	0	g	t_g
	$-9.27 \pm 369j$	0.02	58	$i_{s_d} i_{s_q}\ i_{c_d} i_{c_q}$	$R_g\ k_{ffi}\ R_f$

Modes associated to the grid-forming control.

DC circuit modes.

Modes associated to inductance currents ($\mathbf{i}_{PCC}$).

Aggregated grid related modes.

virtual impedance and a higher damping factor, which is provided by estimating the frequency with a PLL and does not impact the droop response. On the other hand, the dVOC modes show that it is possible to achieve a similar inertial response to SME techniques thanks to the delay added by the first-order filter in the active power. However, the oscillations present a very low damping and it is not possible to attenuate them by modifying the control parameters. In the case of MC, the delivered synthetic inertia is proportional to the energy stored in the dc-link capacitor (Eq. (14)). Therefore, achieving a level of inertia comparable to that of the other techniques would require a large bus capacitor. This fact becomes evident in the behaviour of the modes associated with the GFM control, which exhibit a frequency of oscillation as a consequence of the lower inertia that is higher than in the other cases. Therefore, achieving inertia comparable to the other techniques would require a significantly large bus capacitor.

The modes associated with the electro-mechanical behaviour of the grid are very dependent on the slow dynamics of the turbine and the governor of the network. However, in the case of the MC, the modes associated to the grid oscillate slightly faster, since the converter delivers less synthetic inertia and synchronises faster. On the other hand, the SV, VCVSM, and dVOC exhibit similar oscillation modes related to the dc bus, because they decouple the ac and dc sides by dividing the modulation signal by the bus voltage ($\mathbf{m}_c/v_{dc}$). In the MC, the dc bus voltage v_{dc} determines the electrical frequency behaviour of the grid, resulting in interactions between the ac and dc side. The parametric sensitivity of the eigenvalues associated to θ_c shows that they are strongly linked to the equivalent impedance at the connection node and the *LC* filter. Therefore, if the damping of the MC-controlled converter needs to be improved, the size of the *LC* filter must be modified.

The modes associated with the inductance currents are determined by the synchronous frequency resonance and depend on the equivalent grid impedance $[(R_g + R_f) + j\omega(L_f + L_g)]$ [26]. Analyzing the parametric sensitivities of these modes in the four cases, it can be concluded that the voltage regulator of the inner loops plays an essential role in the dynamics of these modes since it is possible to modify the *LC* filter dynamics through the constants of these regulators. Additionally, these modes are affected by network and filter resistance parameters because they provide damping; however, increasing their values would mean an increase in power losses. The VCVSM resolves this by incorporating a virtual impedance, which modifies the impedance seen by the converter and adding a great versatility over these modes. Regarding the SV, MC and dVOC, they show a lower flexibility to modify these oscillation modes, but e.g. the dVOC achieves a higher damping thanks to its robust voltage control.

5 Parametric sensitivity analysis

In this section a systematic parameter sensitivity analysis for each case is presented. The purpose of the section is twofold: on the one hand, the influence of physical or control parameter variations in the oscillation modes of the system is studied; on the other hand, the performance of the controllers is evaluated for different grid conditions such as aggregated inertia, damping and grid-side impedance.

5.1 Control parameter variation

The first part consists of studying the impact of the control parameters to demonstrate possible ways of tuning each of the grid-forming techniques.

5.1.1 Synchronverter

The synchronverter features a swing equation-based active power regulator that includes a k_d gain for the damping, an inertia constant H and a frequency droop regulator with a k_ω droop gain to mimic the governor of a classical SM.

The parameter K and the reactive power low-pass filter time constant (t_q) are equivalent considering that they act on the reactive power loop dynamics adding a delay on the virtual flux current. The droop parameters k_ω and

k_q define the steady-state behaviour of the active and reactive power and, during transients, they add damping to the critical modes related to grid frequency and currents.

Figure 11 represents the loci of eigenvalues for different parametric sweeps. As the inertia constant H decreases, the dynamics associated to the GFM become faster. However, for very low levels of inertia, the modes related to $\mathbf{i}_{PCC}$ become unstable because the electromechanical dynamics of the converter are in conflict with the inner loops of the converter and the electrical components of the grid. In contrast, high values of inertia constants imply more oscillatory and less damped systems, increasing the time required for the settling between the converter and the grid. Figure 11-b illustrates how, as the damping gain k_d increases, the frequency of the GFM modes raises as well. Finally, the constant K acts as the time constant of a low-pass filter, determining the dynamics of the reactive power loop. Increasing K, the eigenvalue related to i_f slows down and delays the reactive power regulation improving the damping of the modes associated to $\mathbf{i}_{PCC}$.

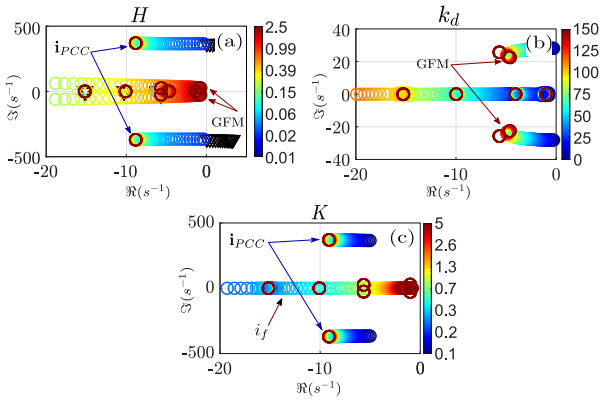

Fig. 11: SV parameter sweep. a) inertia constant (H). b) Damping constant (k_d). c) Constant K.

5.1.2 Voltage-controlled virtual synchronous machine

Figure 12 presents a sweep of the control parameters related to the critical modes of the system. Varying the inertia constant H affects the eigenvalue trajectories as those seen in the SV. However, in this case, varying k_d improves the damping and, thus, the stability margins without affecting the active power-sharing. The reason is that a PLL is used to estimate the grid frequency, meaning that the damping will only react during transients but not affect the steady-state response. This behaviour is more in accordance with the damping effect of a synchronous machine. The virtual impedance values give great flexibility to the VCVSM because as R_v increases, the modes associated to $\mathbf{i}_{PCC}$ move across the real axis. Nonetheless, one limitation is that it affects the behaviour of the voltage in steady-state [27]. As L_v becomes larger, the modes of $\mathbf{i}_{PCC}$ are damped faster, thus, the virtual impedance can be tuned to adjust the position of the eigenvalues related to the synchronous frequency resonance.

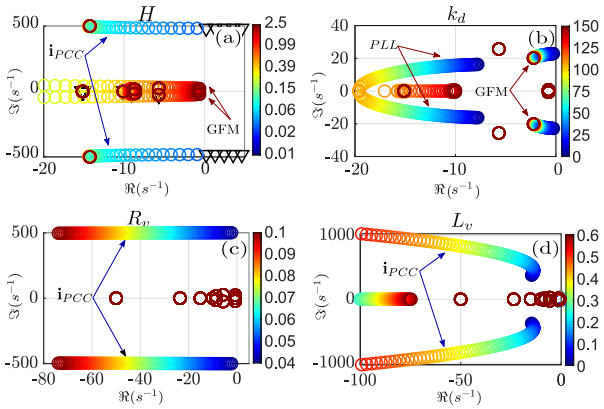

Fig. 12: VCVSM parameter sweep. a) inertia constant (H). b) Damping constant (k_d). c) Virtual resistance (R_v). d) Virtual inductance (L_v).

5.1.3 Matching control

In the MC control the emulated inertia H_{dc} is directly related to the bus capacitor C_{dc} as:

$$H_{dc} = \frac{1}{2}\frac{C_{dc}v_{dc_b}^2}{S_b} \tag{17}$$

where v_{dc_b} is the base dc voltage.

From this equation it can be observed that even for relatively high bus capacitors, the equivalent inertia constant is very low. For instance, for $C_{bus} = 6.28$ p.u., the inertia constant is $H_{dc} = 0.01$ s. Figure 13-a shows the variation of the inertia constant (i.e. the bus capacitor size).

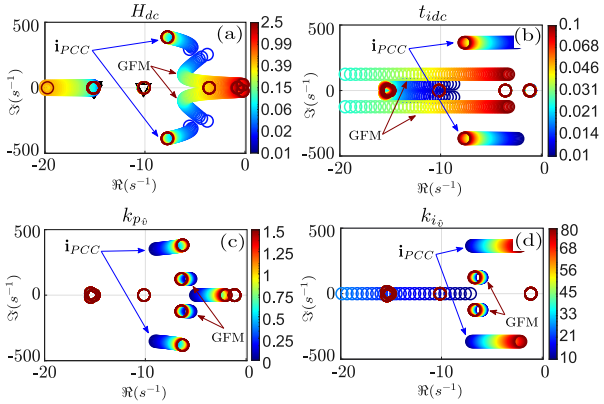

Fig. 13: MC parameter sweep. a) Inertia provided by the dc-bus capacitor (H_{dc}). b) Constant time of the dc source (t_{idc}). c) Proportional gain of the voltage regulator $(k_{p\hat{v}})$. d) Integral gain of the voltage regulator $(k_{i\hat{v}})$.

When the values are low, the GFM-related modes become unstable due to the incapacity of the dc bus to maintain the system frequency. However, the system becomes stable when the inertia constant is $H_{dc} = 0.024$ s ($C_{dc} = 15.07$ p.u.). As the capacitor stores more energy, the system gains damping. However, to improve the RoCoF similar to an SME under the same grid conditions, the inertia constant needs to be around $H_{dc} = 2$ s, which is equivalent to $C_{dc} = 2513$ p.u. Therefore, this type of control exhibits a limitation to emulate a higher inertial behaviour due to the physical constraints with the bus capacitor size. In any case, the dc supply emulates

the response of a governor, so by making the response of this supply faster (i.e. reducing t_{idc}), the GFM could respond more quickly to power imbalances and thus keeping the size of the bus capacitor at more realistic values (Figure 13-b). Concerning the voltage control, the system shows better performance at reduced values of $k_{p_{\hat{v}}}$ and $k_{i\hat{v}}$ (Figure 13-c and d).

5.1.4 Dispatchable virtual oscillator control

The dVOC is composed of the active power droop gain η and a reactive power droop gain α, which at the same time determines the speed of the integrator of $v^*_{o_d}$. As previously mentioned, the dVOC does not provide synthetic inertia to the grid, so the active power filter has an essential role in this control technique since it is the only way to modify the dynamic of the active power delivered by the converter to the grid during transients.

The parametric sweep of the dVOC control parameters shows that the constant η makes the system stable only in a very narrow range of values. When α increases, the mode associated to $v^*_{o_d}$ moves on the real axis, although at the same time, the α-η ratio is lost, and the converter decreases its participation in the regulation of the reactive power. On the other hand, the time constant of the active power filter t_p slows down the mechanical modes but the dominant eigenvalues related to $\mathbf{i}_{PCC}$ increase their speed with the same behaviour of the SME inertia constant (H). In general, the dVOC is modelled as a resonant circuit, and has the advantage of providing a fast and reliable voltage and frequency loop in a way that allows it to respond quickly to changes in the grid. However, the sweep of its parameters reveals the difficulty of improving the damping to the modes related to the GFM control.

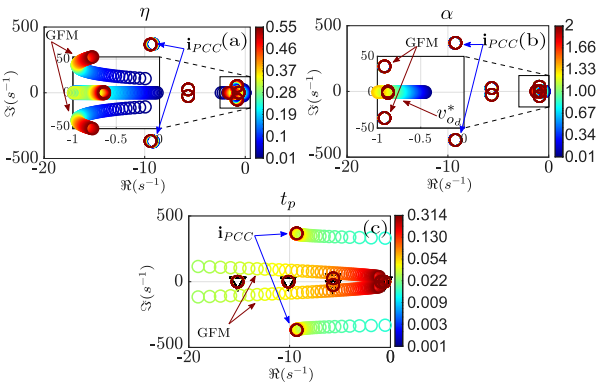

Fig. 14: dVOC parameter sweep. a) (η) gain. b) (α) gain. c) Active power filter time constant (t_p).

5.2 Grid condition variation

Due to all the different devices connected to power systems, their operation points constantly vary, whether due to generation/load variations, contingencies or market operations. In the following sections, a study is carried out to analyse the behaviour of the controllers under various grid conditions. The parameters that are varied include the load power, the grid-side impedance (L_g) and the converter rated power.

5.2.1 Load variation

In an electrical network, the load is one of the most frequently changing variables, which means that the grid operator has to constantly forecast the power demand and ensure an adequate grid operation. To examine the stability of the system against load variations, a sweep of the load resistance connected at the PCC in Figure 1 is carried out. The results in Figure 15 show that the critical modes associated with the PCC currents $\mathbf{i}_{PCC}$ lose damping as the load increases—i.e. as the power consumed by the load increases. This is caused by the damping added by the resistive load. In particular, these modes are slightly affected in the SV, while in the VCVSM and dVOC, they are more dependent on the equivalent impedance in the PCC due to its reactive power regulator. In the MC, the modes related to $\mathbf{i}_{PCC}$ are more sensitive to load variations than the rest of controllers, even to the point of becoming unstable when the load is close to the rated power of the inverter. Likewise, in the MC the modes associated to the GFM have faster dynamics than the other approaches; thus, the equivalent impedance at the PCC strongly affects the behaviour of the grid frequency against power imbalances.

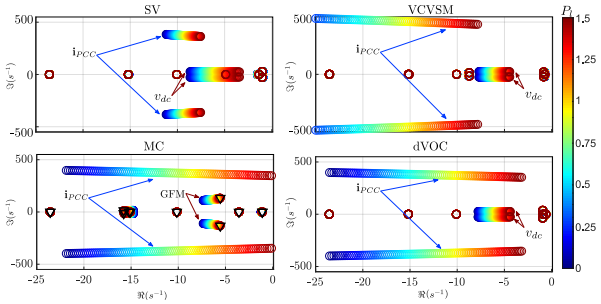

Fig. 15: Eigenvalue trajectory for different load operation points.

5.2.2 Grid-side impedance variation

Several articles in the literature have recently shown that the equivalent grid inductance at the PCC plays a key role in the stability of GFM converters [28, 29]. Figure 16 shows the loci of eigenvalues for variations of the equivalent inductance of the grid (L_g), for each of the GFMs. The results reveal that in all cases, the modes associated with the GFM lose damping at reduced values of L_g since a slight variation in the frequency can lead to a significant increase in the power delivered by the converter. This causes a reduction in the stability margins, and can result in instabilities. The VCVSM achieves a better performance thanks to the virtual inductance (L_v) and the damping term, which improves the damping of the GFM modes as has been previously shown in Figure 12. The SV does not have the same degrees of freedom as the VCVSM and has limitations to increase the damping; this makes the GFM modes more vulnerable to grid-side inductance variations. The dVOC shows unstable points, but this can be solved by changing $\kappa = 0$ to adapt the controller to a resistive line [8]. Concerning the MC, it does not exhibit an electromechanical behaviour with the same time scales as the other controllers. This aspect makes it more susceptible to grid impedance variations.

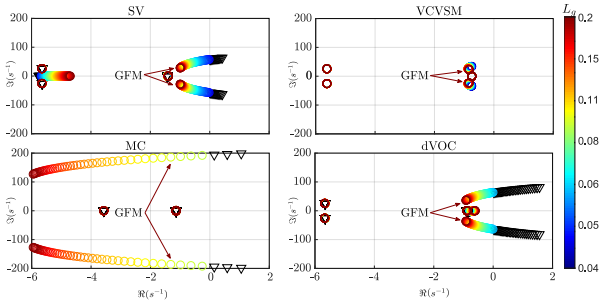

Fig. 16: Eigenvalue trajectory for different grid-side impedance values.

5.2.3 Grid inertia variation

In recent years, the inertial response of power systems has gained importance because the integration of RES into the power system leads to a reduction of the physical inertia connected to the grid, endangering the frequency stability under power disturbances. Figure 17 illustrates the loci of eigenvalues of the four controllers for different inertia values of the grid. The results indicate that the SV achieves a higher damping than the other techniques, since the droop and the damping term changes the power-sharing of the converter in the frequency regulation, causing the converter dynamics to be more dominant and in a higher proportion with respect to the grid. Therefore, the GFM modes are more excited by changes in the network frequency. Regarding VCVSM, MC and dVOC, as the grid delivers higher inertia, the GFM modes become slightly faster, improving the system's stability.

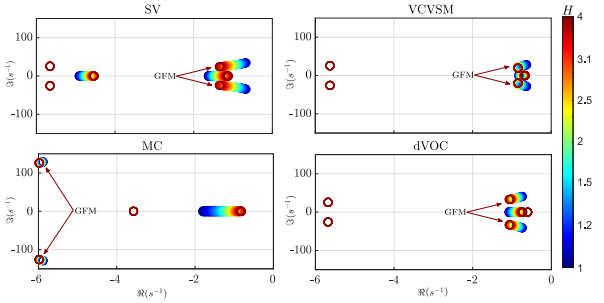

Fig. 17: Eigenvalue trajectory for different grid inertia constants.

5.2.4 Converter rated power variation

As stated above, the number of grid-connected inverters is increasing to the point where a large percentage of generation will be delivered to the grid by electronic converters. Figure 18 depicts the eigenvalues associated to the electromechanical dynamics as the GFM converters change their participation in the system. The parametric sweep consists of modifying the rated power of the inverter, from 0.5 to 1.5 p.u., while keeping the base power (and hence, the grid-side parameters) constant. A modification in the rated power of the inverter impacts not only on the power it provides, but also in the design of the output *LC* filter and the tuning of the inner control loops. When the rated power of the converter is increased, the dominant modes of the SV and VCVSM show a very similar behaviour and move further from the unstable region; hence, these modes gain damping but maintain their oscillation frequency. This response happens because GFM converters provide more damping to the system.

Therefore, it can be stated that the dynamics of the frequency in a low-inertia power system tend to improve with a higher penetration of GFM converters.The MC moves its modes in the same direction as the SME, although it gains more damping due to the rise in R_f filter resistance. Regarding the dVOC, its eigenvalues move differently from the SV, VCVSM and MC control due to the difficulty of the controller to providing damping to the grid. Anyhow, the conclusion is that the power ratio is not a critical source of instability in the tested scenario.

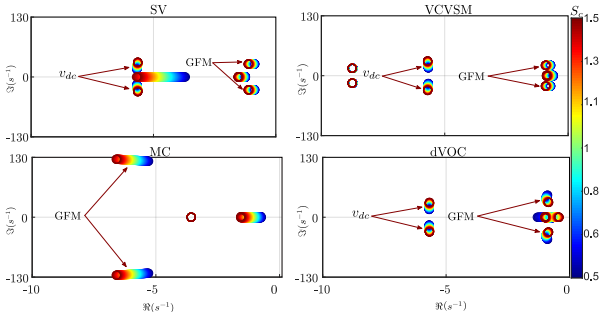

Fig. 18: Eigenvalue trajectory for a parametric sweep of the converter rated power for the four implementations.

6 Real-Time Implementation and Validation

In order to validate the proposed small-signal models and the subsequent stability analysis, a hardware-in-the-loop (HIL) testbed based on an OPAL-RT as shown in Figure 19 has been used. The semiconductors of the converter, the *LC* filter, the load and the synchronous machine have been implemented on this OPAL-RT, whereas the grid-forming control, inner loops and space vector modulation (SVPWM) have been integrated on a TMS320F28379D launchpad from Texas Instruments.

Fig. 19: Opal-RT based real-time HIL testbed.

The experimental results in Figure 20 show that with a variation of 0.05 p.u in the active power reference of the converter, the real-time simulations show a very similar behaviour in the frequency and amplitude of the power oscillations compared to the small-signal models. Moreover, despite the 0.02 p.u. ripple in the HIL testbed caused by the converter switching, the results converge to the same operating point in steady-state. The only difference between experimental and small-signal simulation results are observed in the amplitude of the oscillations of the

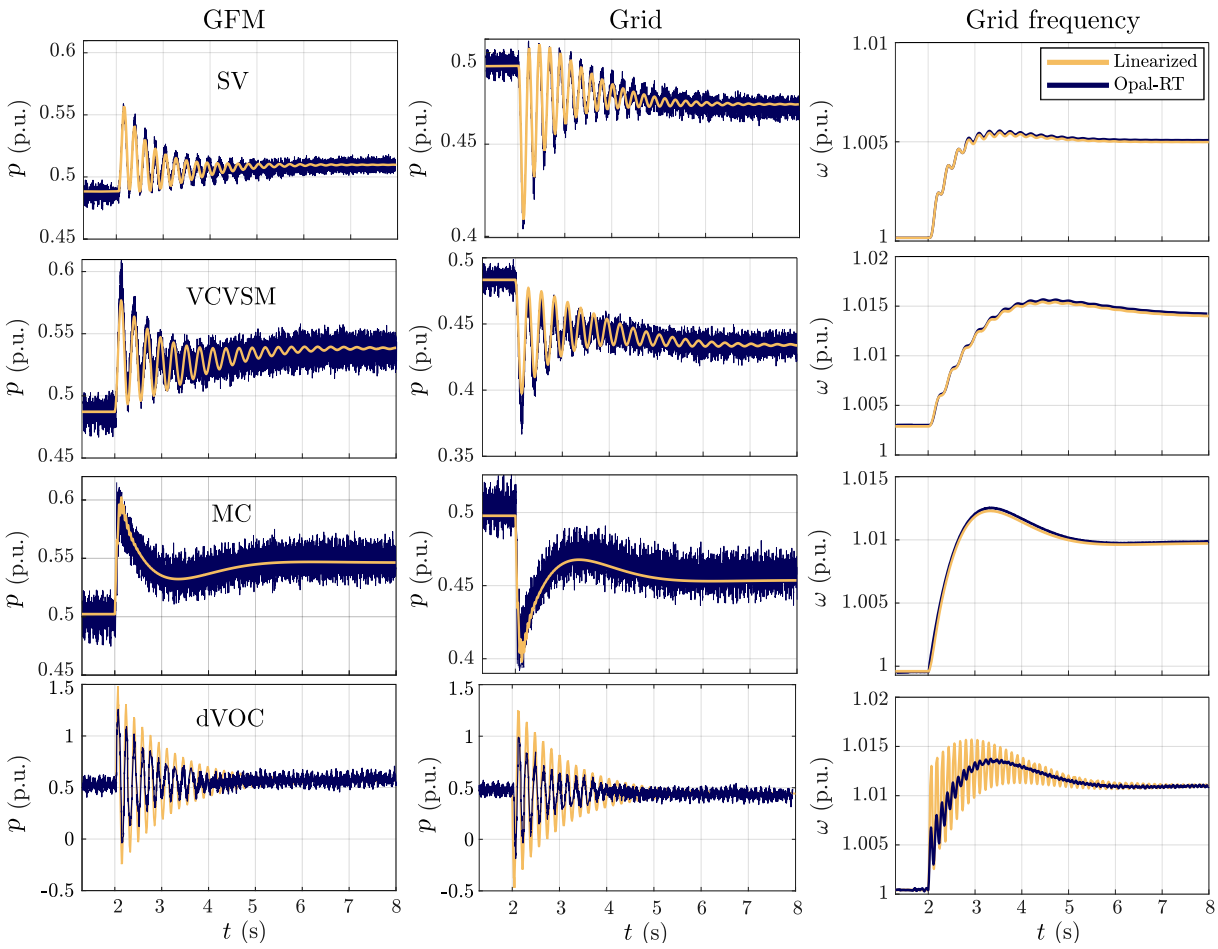

Fig. 20: Validation of the linearized model against real-time simulation based on Opal-RT. From left to right, GFM power, SM power and grid frequency in each case.

dVOC. This is due to the large amplitude of these oscillations, that saturates the currents and voltage measurements of the experimental setup. This saturation has not been considered in the analytical small-signal model. In any case, the frequency of the oscillations is the same both for the simulation and for the experimental results.

7 Conclusions

This paper has studied and compared the time-domain and small-signal behaviour of four of the most relevant grid-forming control implementations: a synchronverter, a voltage-controlled virtual synchronous machine, a dispatchable virtual oscillator, and a matching control. Unlike previous studies in the literature, the performance of the controllers has been tested for varying grid conditions such as the equivalent inertia constant, damping and grid-side impedance.

The results reveal that the dVOC has similar inertial behaviour to the SV and the VCVSM when a low-pass filter is added to the active power measurement, since the time constant of the filter is equivalent to the inertial term of the swing equation. However, the dVOC does not have a damping term that allows attenuation of modes associated to the electromechanical response of the converter. The MC presents some challenges because the provided inertial behaviour depends directly on the size of the bus capacitor, and its stability is strongly dependent on the passive

elements of the system. The VCVSM is a more reliable representation of the synchronous machine, allowing better attenuation of electromechanical oscillations thanks to its damping term. In contrast, the SV does not correctly represent the damping term in variable frequency grids, impacting the active power-sharing concerning the rest of the generators in the system.

Regarding reactive power regulation, the VCVSM provides more flexibility due to the integration of a virtual impedance, allowing the GFM converter to operate even in very low-impedance grids. Nevertheless, its stability is sensitive to the droop gain of the reactive power, which is better, e.g. in the reactive power loop of the SV. The dVOC exhibits faster and more robust reactive power control that does not affect stability with its reactive power droop gain.

The final experimental results have shown a good match with the response of the developed analytical models, corroborating the validity of the results in the study of the small-signal stability.

References

[1] J. O'Sullivan, A. Rogers, D. Flynn, P. Smith, A. Mullane, and M. O'Malley, "Studying the Maximum Instantaneous Non-Synchronous Generation in an Island System-Frequency Stability Challenges in Ireland," *IEEE Trans. Power Syst.*, vol. 29, no. 6, pp. 2943–2951, 2014.

[2] U. Markovic, O. Stanojev, P. Aristidou, E. Vrettos, D. S. Callaway, and G. Hug, "Understanding Small-Signal Stability of Low-Inertia Systems," *IEEE Trans. Power Syst.*, p. 1, 2021.

[3] T. L. Vandoorn, J. D. M. De Kooning, B. Meersman, and L. Vandevelde, "Review of primary control strategies for islanded microgrids with power-electronic interfaces," *Renew. Sustain. Energy Rev.*, vol. 19, pp. 613–628, 2013.

[4] J. M. Guerrero, J. C. Vasquez, and R. Teodorescu, "Hierarchical control of droop-controlled DC and AC microgrids - a general approach towards standardization," *2009 35th Annu. Conf. IEEE Ind. Electron.*, pp. 4305–4310, 2009.

[5] E. Unamuno, J. A. Suul, M. Molinas, and J. A. Barrena, "Comparative Eigenvalue Analysis of Synchronous Machine Emulations and Synchronous Machines," in *IECON 2019 - 45th Annu. Conf. IEEE Ind. Electron. Soc.*, vol. 1, 2019, pp. 3863–3870.

[6] T. Jouini, C. Arghir, and F. Dörfler, "Grid-Friendly Matching of Synchronous Machines by Tapping into the DC Storage," *IFAC-PapersOnLine*, vol. 49, no. 22, pp. 192–197, 2016.

[7] B. B. Johnson, M. Sinha, N. G. Ainsworth, F. Dörfler, and S. V. Dhople, "Synthesizing Virtual Oscillators to Control Islanded Inverters," *IEEE Trans. Power Electron.*, vol. 31, no. 8, pp. 6002–6015, 2016.

[8] G.-S. Seo, M. Colombino, I. Subotic, B. Johnson, D. Groß, and F. Dörfler, "Dispatchable Virtual Oscillator Control for Decentralized Inverter-dominated Power Systems: Analysis and Experiments," *2019 IEEE Appl. Power Electron. Conf. Expo.*, pp. 561–566, 2019.

[9] S. D'Arco and J. A. Suul, "Equivalence of Virtual Synchronous Machines and Frequency-Droops for Converter-Based MicroGrids," *IEEE Trans. Smart Grid*, vol. 5, no. 1, pp. 394–395, 2014.

[10] O. Mo, S. D'Arco, and J. A. Suul, "Evaluation of Virtual Synchronous Machines With Dynamic or Quasi-Stationary Machine Models," *IEEE Trans. Ind. Electron.*, vol. 64, no. 7, pp. 5952–5962, 2017.

[11] O. Saborío, "Small-signal modelling and stability analysis of a traditional generation unit and a virtual synchronous machine in grid- connected operation," 2015.

[12] N. Pogaku, M. Prodanovic, and T. C. Green, "Modeling, analysis and testing of autonomous operation of an inverter-based microgrid," *IEEE Transactions on Power Electronics*, vol. 22, no. 2, pp. 613–625, 2007.

[13] A. Tayyebi, D. Groß, A. Anta, F. Kupzog, and F. Dörfler, "Frequency Stability of Synchronous Machines and Grid-Forming Power Converters," *IEEE J. Emerg. Sel. Top. Power Electron.*, vol. 8, no. 2, pp. 1004–1018, 2020.

[14] Y. Lin, B. Johnson, V. Gevorgian, V. Purba, and S. Dhople, "Stability assessment of a system comprising a single machine and inverter with scalable ratings," in *2017 North American Power Symposium (NAPS)*, 2017, pp. 1–6.

[15] M. M. Siraj Khan, Y. Lin, B. Johnson, M. Sinha, and S. Dhople, "Stability assessment of a system comprising a single machine and a virtual oscillator controlled inverter with scalable ratings," in *IECON 2018 - 44th Annual Conference of the IEEE Industrial Electronics Society*, 2018, pp. 4057–4062.

[16] P. Kundur, *Power system stability and control*, ser. The EPRI Power System Engineering Series. New York [etc: McGraw-Hill, 1994.

[17] D. Pan, X. Wang, F. Liu, and R. Shi, "Transient Stability of Voltage-Source Converters With Grid-Forming Control: A Design-Oriented Study," *IEEE J. Emerg. Sel. Top. Power Electron.*, vol. 8, no. 2, pp. 1019–1033, 2020.

[18] L. Huang, H. Xin, Z. Wang, K. Wu, H. Wang, J. Hu, and C. Lu, "A Virtual Synchronous Control for Voltage-Source Converters Utilizing Dynamics of DC-Link Capacitor to Realize Self-Synchronization," *IEEE J. Emerg. Sel. Top. Power Electron.*, vol. 5, no. 4, pp. 1565–1577, 2017.

[19] Q.-C. Zhong, P.-L. Nguyen, Z. Ma, and W. Sheng, "Self-Synchronized Synchronverters: Inverters Without a Dedicated Synchronization Unit," *IEEE Trans. Power Electron.*, vol. 29, no. 2, pp. 617–630, 2014.

[20] I. Cvetkovic, D. Boroyevich, R. Burgos, C. Li, and P. Mattavelli, "Modeling and control of grid-connected voltage-source converters emulating isotropic and anisotropic synchronous machines," *2015 IEEE 16th Work. Control Model. Power Electron.*, pp. 1–5, 2015.

[21] C. Arghir and F. Dörfler, "The Electronic Realization of Synchronous Machines: Model Matching, Angle Tracking, and Energy Shaping Techniques," *IEEE Trans. Power Electron.*, vol. 35, no. 4, pp. 4398–4410, 2020.

[22] C. Arghir, T. Jouini, and F. Dörfler, "Grid-forming control for power converters based on matching of synchronous machines," *Automatica*, vol. 95, pp. 273–282, 2018.

[23] M. Colombino, D. Groß, J.-S. Brouillon, and F. Dörfler, "Global Phase and Magnitude Synchronization of Coupled Oscillators With Application to the Control of Grid-Forming Power Inverters," *IEEE Trans. Automat. Contr.*, vol. 64, no. 11, pp. 4496–4511, 2019.

[24] D. Serrano-Jiménez, E. Unamuno, A. G. de Muro, D. Aragon, S. Ceballos, and J. Barrena, "Stability tool for electric power systems with a high penetration of electronic power converters," *Electric Power Systems Research*, vol. 210, p. 108115, 2022.

[25] S. D'Arco, J. A. Suul, and O. B. Fosso, "Automatic Tuning of Cascaded Controllers for Power Converters Using Eigenvalue Parametric Sensitivities," *IEEE Trans. Ind. Appl.*, vol. 51, no. 2, pp. 1743–1753, 2015.

[26] J. Wang, Y. Wang, Y. Gu, W. Li, and X. He, "Synchronous frequency resonance of virtual synchronous generators and damping control," in *2015 9th International Conference on Power Electronics and ECCE Asia (ICPE-ECCE Asia)*, 2015, pp. 1011–1016.

[27] E. Unamuno, J. Paniagua, and J. A. Barrena, "Unified Virtual Inertia for ac and dc Microgrids: And the Role of Interlinking Converters," *IEEE Electrif. Mag.*, vol. 7, no. 4, pp. 56–68, 2019.

[28] X. Wang, M. G. Taul, H. Wu, Y. Liao, F. Blaabjerg, and L. Harnefors, "Grid-synchronization stability of converter-based resources−an overview," *IEEE Open Journal of Industry Applications*, vol. 1, pp. 115–134, 2020.

[29] Y. Li, Y. Gu, and T. Green, "Revisiting grid-forming and grid-following inverters: A duality theory," *IEEE Transactions on Power Systems*, pp. 1–1, 2022.